A LOW-ENERGY MULTIHOLE CONVERGING COLLIMATOR COMPARED WITH A PINHOLE COLLIMATOR

R. A. Moyer

Searle Radiographics Inc., Des Plaines, Illinois

It is apparent from the equations describing the performance of the pinhole and converging collimators on the scintillation camera that the sensitivity, resolution, and field of view of these two collimators are very different as a function of distance from the collimator face. A 6,000-hole converging collimator designed for ^{99m}Tc having a 15-cm field of view diameter at 10 cm from the collimator face was constructed and compared with the Searle Radiographics pinhole collimator. The sensitivity of the converging collimator increases with depth while that of the pinhole collimator decreases. The resolution of the collimator-camera system degrades more rapidly with depth for the pinhole collimator. The field of view of the converging collimator decreases with increasing object-to-collimator distances while that of the pinhole collimator increases with depth. The experimental results agree with the derived equations and imply that the converging collimator has very different performance characteristics from the pinhole collimator and that it should be useful in the imaging of small organs.

In 1968 Beck (*1*) suggested construction of a converging collimator specifically for thyroid imaging. Recently there has been a growing interest (*2–5*) in the application of converging collimators to cardiac, pediatric, and renal studies.

Because of the inherent magnification properties of converging collimators, the relative contribution of intrinsic camera resolution to total system resolution is reduced in inverse proportion to the magnification factor. A similar factor appears in the efficiency calculation. Thus one obtains improved system resolution and increased collimator efficiency at the expense of decreased field size over comparably designed parallel-hole collimators.

A converging collimator used on a scintillation camera should be useful for any study which fits within the field of view of the collimator. Since few converging collimators exist, inverting the medium-energy diverging collimator* has occasionally been suggested to obtain a converging collimator (*6*). With the new advances in camera performance, the individual collimator holes are usually visible in scintiphotos taken using inverted medium-energy diverging collimators. Thus the need for a low-energy converging collimator is readily apparent.

Many of the same objectives (high resolution, high efficiency, and smaller field of view) can be obtained with the pinhole collimator. It thus becomes necessary to compare the pinhole and converging collimators and distinguish any differences between the two.

In some respects a converging collimator is similar to a pinhole collimator; however, the pinhole collimator suffers from rapidly changing field of view with distance. This effect produces changes in resolution and efficiency which sometimes introduce objectionable distortions into scintiphotos.

PERFORMANCE

The prediction of pinhole collimator performance has been developed through the work of Anger and Rosenthal (*7*), Mallard and Myers (*8*), Anger (*9*), and Paix (*10*). Rather than reproduce their derivations here, only the results will be presented with reference to Fig. 1.

The geometric efficiency of a pinhole collimator for a point source has been expressed (*9*) in terms of the dimensions b, d_e and θ shown in Fig. 1 as

$$g = \frac{d_e^2 \sin^3 \theta}{16b^2}, \qquad (1)$$

Received Aug. 10, 1973; original accepted Aug. 21, 1973.

For reprints contact: R. A. Moyer, Searle Radiographics Inc., 2000 Nuclear Dr., Des Plaines, Ill. 60018.

* Searle Radiographics Part No. 821516.

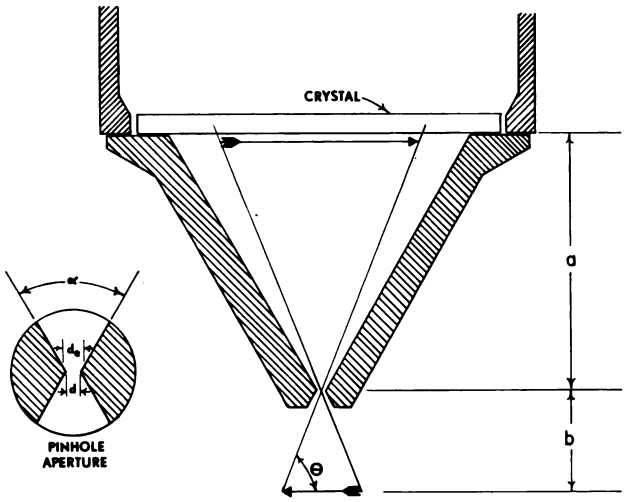

FIG. 1. Single pinhole collimator showing inversion of image and symbols used in describing efficiency and resolution. Insert shows aperture and related symbols in greater detail.

where the efficiency, g, is defined as the fraction of gamma rays emitted by a point source which passes through the aperture and strikes the crystal. The effective diameter, d_e, is larger than the physical diameter, d, of the aperture. The effective diameter is an approximation to account for penetration of gamma rays through the edge of the aperture. It is given by $d_e = [d(d + 2\mu^{-1} \tan \alpha/2)]^{1/2}$ where μ^{-1} is mean free path of gamma rays in the collimator material.

Resolution of the pinhole collimator in the object plane, R_p, is given by

$$R_p = \frac{(a + b)d_e}{a}. \qquad (2)$$

R_p is the distance between two point sources in the object plane that are imaged as tangential disks in the crystal. As discussed later, it is very difficult to measure R_p experimentally. The overall system resolution in the object plane includes the magnification factor, b/a, given by

$$R_s = \sqrt{R_p^2 + [(b/a)R_i]^2}, \qquad (3)$$

where R_i is the intrinsic camera resolution without a collimator. Note that the magnification factor reduces the effective contribution of intrinsic resolution to overall system resolution when b is less than a.

Important points to note from the above equations are that the efficiency is not constant throughout the plane at a fixed distance from the aperture and that the efficiency and resolution both become worse with increasing distances from the aperture.

Little work has been done on formulation of a theory to predict the performance of multihole converging collimators. To fill this deficiency a derivation similar to that used in the theory of diverging collimators (*11*) is given below for the efficiency and resolution of converging collimators.

First, the derivation of the efficiency of parallel multihole collimators will be reviewed. The efficiency of such collimators to either a point source or extended plane source which lies within the field of view of the collimator is obtained by considering the product of two factors: (A) the solid angle subtended by an individual hole (area of hole divided by $4\pi a^2$ is a good approximation for long collimators with narrow holes), and (B) the lead-to-air ratio of a unit cell. Translated into an equation this becomes

$$g_0 = \frac{\text{Area of hole at crystal side}}{4\pi a_e^2} \times \frac{\text{Area of hole at patient side}}{\text{Area of unit cell}} \qquad (4)$$

where a_e is the effective collimator length which has been reduced from the actual length, a, because of septum penetration at both ends of the holes and is given (*9*) approximately by $a_e = a - 2\mu^{-1}$. For round holes (inner diameter d and minimum septum thickness t) in a hexagonal array, Eq. 4 can be written as

$$g_0 = \frac{\pi(d/2)^2}{4\pi a_e^2} \times \frac{2\pi(d/2)^2}{(3)^{1/2}(d + t)^2} \qquad (5)$$

where the unit cell is a hexagon of dimensions d + t across the flats.

Because of the magnifying properties of a converging collimator, an additional term is needed in Eqs. 4 and 5. The justification for this term is shown in Fig. 2 where f is the collimator focal distance (distance from focus point to nearest collimator face), A and A′ are the areas viewed by the collimator at a distance b and against the collimator face, respectively. As long as the source is within the field of view of the collimator, a source of area A at different distances, b, acts as though it has an effective area, A′, against the collimator face. The relation between the two areas from the geometry of Fig. 2 is

$$\frac{A}{A'} = \frac{(f - b)^2}{f^2}. \qquad (6)$$

The slanting holes (Fig. 3) of the converging collimator require that the a_e of Eq. 4 be further modified to $a'_e = a_e/\cos \theta$. The factor $\cos \theta$ takes into account the increased length of each hole which is not on the central axis. The efficiency for converging collimators then becomes

$$g = g'_0 \times \frac{f^2}{(f - b)^2} \qquad (7)$$

where g'_0 is the g_0 of Eq. 5 with a_e replaced by a'_e.

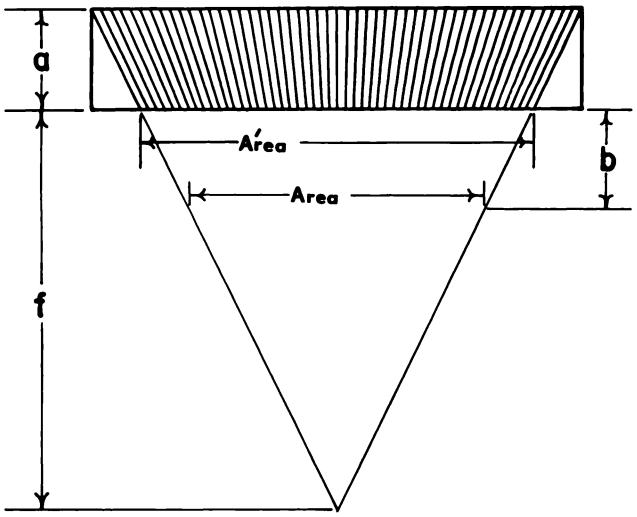

FIG. 2. Converging collimator detailing field of view in terms of area against collimator face and at distance, b, from collimator face.

Note that in the above expression, efficiency increases with increasing distance from the collimator face which is in contrast to the efficiency of the pinhole collimator.

The angle θ of Fig. 1 is not the same as that of Fig. 3. Realizing this and using the θ of Fig. 3, the efficiency variation across a plane at a fixed distance from the pinhole aperture is proportional to $\cos^3 \theta$. A similar variation in the converging collimator is proportional to $\cos^2 \theta$. The typical range of θ values for the pinhole collimator is 0–32 deg, while for the experimental converging collimator (Table 1) θ ranges from 0 to 17 deg. Hence, the converging collimator has a much better uniformity of efficiency across its field of view.

The resolution of a converging collimator can be calculated by using the general method described by Anger (*12*) where the half height of the response to a point source is calculated assuming that the collimator moves. The half height, R, in the crystal plane (from Fig. 3) is given by

$$R = AB + BC = (a_e + b + c)(\tan \alpha + \tan \theta') \quad (8)$$

where a_e takes into account the septum penetration at the ends of each hole. Using the smaller triangles with included angles α and θ in the rightmost collimator hole of Fig. 3, R can be expressed as

$$R = \frac{(a_e + b + c)}{a_e} \times \frac{d}{\cos \theta} + (a_e + b + c)(\tan \theta' - \tan \theta). \quad (9)$$

Resolution can be expressed in terms of focal length and resolution in the object plane, R_0. This resolution, R_0, is calculated for the plane of the object and not in the crystal plane as was done in Eqs. 8 and 9. For parallel-hole collimators R and R_0 are equal, while for converging collimators they are related by

$$R_0 = M_c R \quad (10)$$

where M_c is the minification factor for the converging collimator,

$$M_c = (f - b)/(f + a_e + c). \quad (11)$$

From the larger portion of Fig. 3,

$$R = AD + DC, \quad (12)$$

where DC can be expressed as

$$DC = (f + a_e + c)(\tan \theta' - \tan \theta). \quad (13)$$

From similar triangles in the rightmost collimator hole of Fig. 3,

$$AD = \frac{(a_e/2 + c)d}{a_e \cos \theta}. \quad (14)$$

From the above Eqs. 10–14, R_0 can be expressed as

$$R_0 = \frac{(a_e + b + c)d}{a_e} \times \frac{1}{\cos \theta}\left[1 - \frac{c + a_e/2}{f + a_e + c}\right]. \quad (15)$$

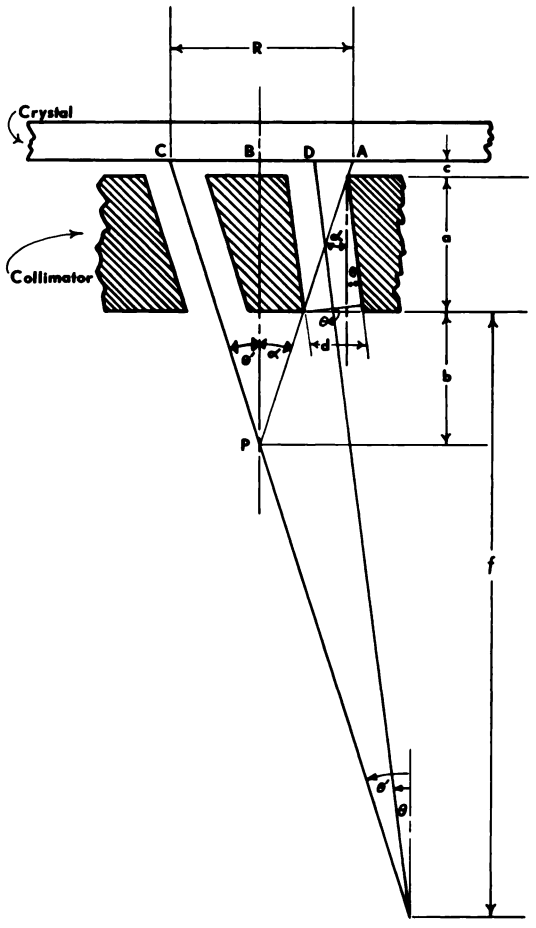

FIG. 3. Detail of two holes of converging collimator and crystal assembly showing symbols used in derivation of efficiency and resolution.

Equation 15 can be thought of as combining three terms: the first, $(a_e + b + c)d/a_e$ is the conventional equation for resolution of parallel-hole collimators (*9,12*), the second $1/\cos\theta$ is an additional term due to the slant of the holes, while the term in brackets is due to the effect of all holes focusing to a point.

COMPARISON WITH PINHOLE COLLIMATOR

Plotted in Figs. 4 and 5 are experimental efficiency and resolution data for the collimators of dimensions given in Table 1. The solid lines in these figures are smooth curves drawn through the experimental data points to aid the eye. The predicted values for the converging collimator using Eqs. 7 and 15 adjusted for triangular hole shape are indicated by the dashed curves. The experimental data points for the converging collimator are denoted by the encircled data points. Figure 6 shows the variation in field of view with distance from each of the collimators as calculated from the collimator dimensions and focal length where applicable. Two orientations of the pinhole collimator* are listed in Table 1. "Long" refers the way the 5½-in.-diam insert is attached in such a manner that the shiny side is toward the patient and the aperture is at a maximum distance from the crystal. In the "short" configuration the dull, concave lead side is facing the patient and the aperture is at minimum distance from the crystal. Efficiency data have been normalized to that of the 4,000-hole parallel-hole collimator† at 4 in. since this collimator has been widely used in the past.

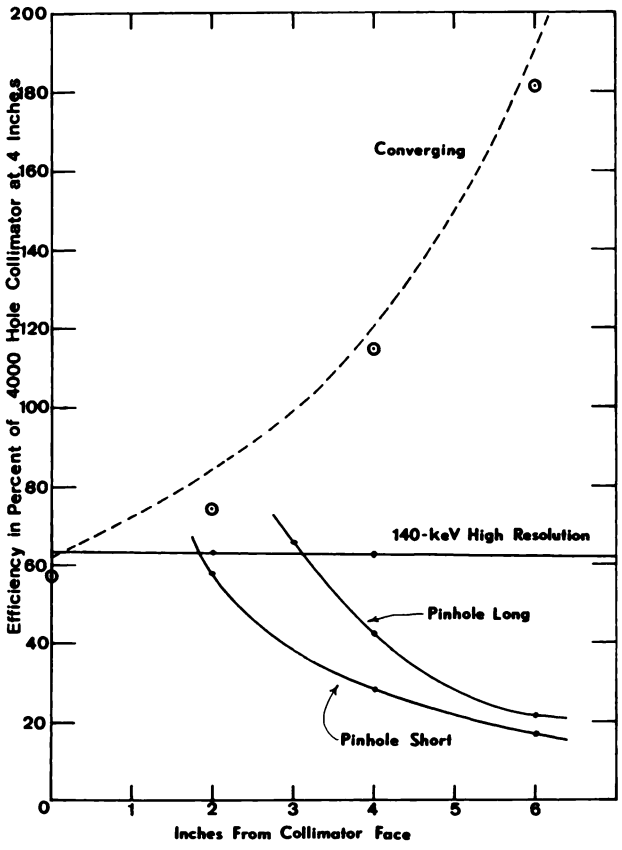

FIG. 4. Relative efficiency of collimators studied for 140-keV gamma rays of ^{99m}Tc in air. Solid curves have been drawn through experimental data points to aid eye. Dashed curve represents predicted values for converging collimator from Eq. 7 using parameters of Table 1. Encircled data points are experimental data for converging collimator. Note very different variation in efficiency with depth for pinhole and converging collimator.

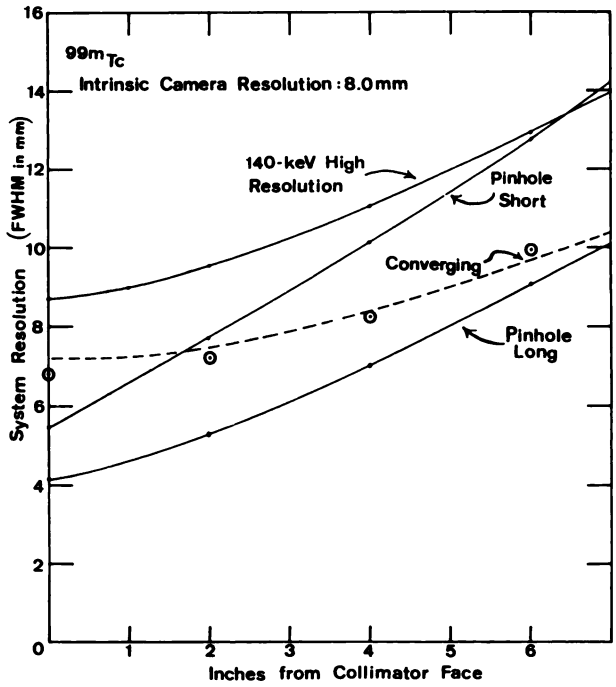

FIG. 5. System resolution (FWHM of line source) in air of collimators studied for 140-keV gamma rays of ^{99m}Tc on scintillation camera having an 8.0-mm intrinsic resolution. Solid curves have been drawn through experimental data points to aid eye. Dashed curve is predicted values of system resolution for converging collimator using parameters of Table 1 and summing in quadrature R_0 of Eq. 15 and product of minification factor times intrinsic camera resolution. Encircled data points are experimental data for converging collimator.

The increase in efficiency with increasing collimator-to-patient separation for the converging collimator is very apparent from Fig. 4. Note that the pinhole has decreasing efficiency with increased collimator-to-patient separation, b, as expected from Eq. 1. The formula for efficiency of parallel-hole collimators predicts that efficiency should be independent of depth.

The experimental data shown in Fig. 4 are for a disk source approximately 3 in. in diameter. Hence, these data give little indication of the radial dependence in efficiency of the pinhole and converging collimators previously discussed in the performance section.

* Searle Radiographics Part No. 820718.

† Searle Radiographics Part No. 820719.

TABLE 1. COLLIMATOR DIMENSIONS

Collimator	Number of holes	Center hole shape	Focal length (in.)	Collimator length (in.)	Center hole diameter (in.)	Septum thickness (in.)	C* dimension (in.) (140 keV)
Single pinhole	1	Round		—Long—	0.187	—	7.89†
Single pinhole	1	Round		—Short—	0.187	—	5.90†
140-keV high resolution	~15,000	Triangular	—	1.160	h 0.075‡ b 0.105	0.010	0.380
Experimental converging	~6,000	Triangular	13.75	2.5	h 0.107‖ b 0.161	0.010	0.380

* C is distance from collimator to crystal interaction plane (140 keV). Interaction is assumed to take place 0.125 in. inside crystal.
† Distance from aperture to crystal interaction plane.
‡ h = inside height of triangle; b = inside base of triangle.
‖ Dimensions for narrow end of triangular hole (towards patient).

The effect of gamma-ray attenuation in the patient is not included in Figs. 4 and 5 since all measurements were made in air. The thickness of tissue (water) necessary to absorb half of the gamma rays emitted by ^{99m}Tc is approximately 1.8 in. In the clinical situation, attenuation by the patient is present and effectively reduces the efficiency of the converging collimator with depth from that shown in Fig. 4. This would tend to lessen any counting rate variation with depth observed using the converging collimator; while for the pinhole collimator, the same effect would accentuate that collimator's counting rate variation with depth.

As can be seen from Fig. 5, the degradation of resolution with distance from the converging collimator face is much less than that for either of the two pinhole collimator configurations and for the high-resolution collimator. This is caused by the cancellation of two effects. The first is the normal degradation of collimator resolution as one moves the object further away from the collimator. This effect is offset, however, by a second effect, namely the increased magnification (and thus lower effective contribution of intrinsic camera resolution) obtained as the object approaches the focal point of the converging collimator.

Figure 6 shows another basic difference between the converging and pinhole collimators. The rapidly changing field of view in the pinhole collimator causes underlying structures to be "condensed" and thus for short patient-to-collimator distances, this effect may yield scintiphotos which are sometimes difficult to interpret for clinicians inexperienced in its use. The converging collimator will cause underlying structures to be "spread out." The changing image size is not as rapid in the case of the converging collimator as it is for the pinhole collimator.

The measured resolution (Fig. 5) for the two configurations of the pinhole collimator is considerably

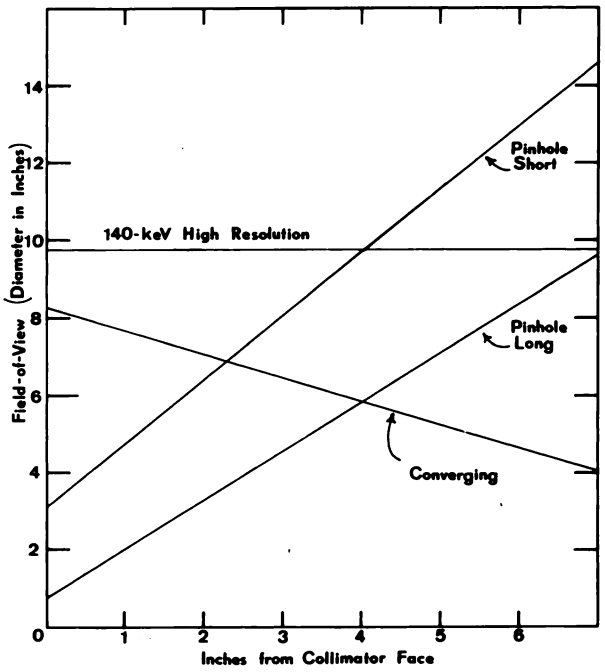

FIG. 6. Field of view for collimators listed in Table 1 as function of depth. Variation in field of view with depth is markedly different for pinhole and converging collimator.

better than that calculated from Eqs. 2 and 3 using the data of Table 1. This is due to the fact that the measured resolution is the full width at half maximum (FWHM) of a line source, whereas, R_p as derived in Ref. 9 is related to the minimum separation of two point sources in the object plane that are imaged as tangential disks in the crystal. R_p is thus somewhat like a full width at full maximum but since the disk response function is not Gaussian in shape, any simple calculation of FWHM is expected to be in error. Nonetheless, Eqs. 2 and 3 are valuable since they do indicate the dependence of R_p and R_s on the crystal-aperture distance, aperture-patient distance, and size of the aperture.

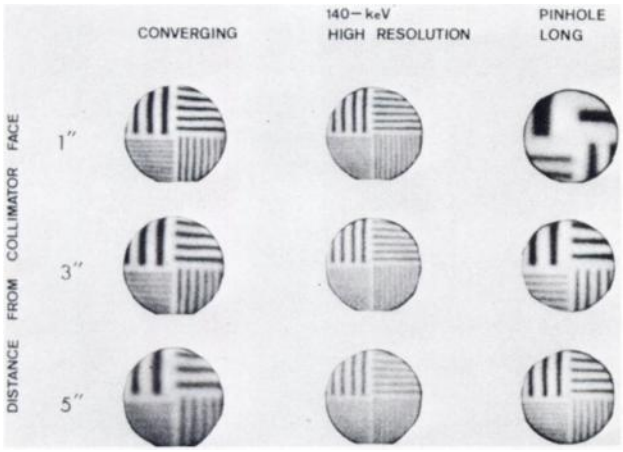

FIG. 7. Scintiphotos of bar phantoms in air at various distances from respective collimator face. Phantom consists of alternating bars and spaces of 3/16, 1/4, 3/8, and 1/2 in. No distortion is evident in any of scintiphotos. Magnification of pinhole collimator increases very rapidly as object approaches collimator face.

Scintiphotos illustrating the changing resolution and field of view with depth for pinhole, converging, and high-resolution collimators are shown in Fig. 7. The resolution pattern in these pictures is that of alternating bars and spaces of $\frac{3}{16}$, $\frac{1}{4}$, $\frac{3}{8}$, and $\frac{1}{2}$ in. Only scintiphotos for the long configuration of the pinhole collimator are shown since it has better resolution and efficiency (at the sacrifice of field of view) than the short configuration. The variation with depth of efficiency, resolution, and field of view are quite similar for the short and long configurations. It should be noted that for the pinhole collimator, the axes of Figs. 4–6 and depth indicated in Fig. 7 are measured from the farthest protruding surface of the collimator and not from the aperture.

It should be further noted that there is no spatial distortion in each plane at a fixed depth for any of the collimators in Fig. 7. Distortion will occur when an object of finite thickness is imaged and then it will be a complicated function of the efficiency, resolution, and field of view of each collimator.

From Fig. 4–7 it is quite apparent that a properly designed converging collimator is desirable for imaging small organs. The converging and pinhole collimators have very different performance characteristics, particularly in the variation of efficiency and field of view with distance from the collimator face. The result of these effects combined with anatomical structure is expected to give quite different scintiphotos for the two collimators in clinical situations. A clinical comparison study between the pinhole collimator and the converging collimator should be undertaken to determine whether a converging collimator will become the collimator of choice for small organ studies.

The performance of the converging collimator as predicted from Eq. 7 and 15 is in good agreement with the experimental results as indicated in Fig. 4 and 5. This indicates the validity of the derivations in the performance section of this paper. Thus by using Eq. 7 and 15 one can design other converging collimators or the modification of existing collimators.

Inverted diverging collimators do not fully use the advantages of the increased resolution and efficiency which would result from shorter focal lengths. This suggests the need for converging collimators which are designed specifically for that use and not just inverted diverging collimators. The converging collimator described in this article is undergoing clinical evaluation to see if it satisfies the clinical requirements for such a collimator.

ACKNOWLEDGMENT

The author wishes to thank G. Muehllehner for many helpful discussions and suggestions during the preparation of this manuscript, and both J. H. Dudek and A. M. Smudde for the preparation of the figures.

REFERENCES

1. BECK RN: Collimation of gamma rays. In *Fundamental Problems in Scanning*, Gottschalk A, Beck RN, eds, Springfield, Ill, CC Thomas, 1968, pp 71–92

2. DOWDEY JE, GRAHAM KD, BONTE FJ: Collimator magnification of scintillation camera images. *J Nucl Med* 12: 352, 1971

3. RUDIN S, BARDFELD PA, HART H: Use of magnifying multihole collimators in the gamma-ray camera system. *J Nucl Med* 12: 831–834, 1971

4. RUDIN S, RIDER KL, HART HE: A tomographic magnifying collimator system for the gamma camera. *Radiology* 102: 371–373, 1972

5. DOWDEY JE, BONTE FJ: Principles of scintillation camera image magnification with convergent collimators. *Radiology* 104: 89–96, 1972

6. LORENZ WJ, SCHMIDLIN P, KAMPMANN H, et al: Comparative investigations with the Anger scintillation camera and the digital autofluoroscope. In *Medical Radioisotope Scintigraphy*, vol 1, Vienna, IAEA, 1969, pp 135–143

7. ANGER HO, ROSENTHAL DJ: Scintillation camera and positron camera. In *Medical Radioisotope Scanning*, Vienna, IAEA, 1959, pp 59–75

8. MALLARD JR, MYERS MJ: The performance of a gamma camera for the visualization of radioactive isotope in vivo. *Phys Med Biol* 8: 165–182, 1963

9. ANGER HO: Radioisotope cameras. In *Instrumentation in Nuclear Medicine*, vol 1, Hine GJ, ed, New York, Academic Press, 1967, pp 485–552

10. PAIX D: Pinhole imaging of gamma rays. *Phys Med Biol* 12: 489–500, 1967

11. MUEHLLEHNER G: A diverging collimator for gamma-ray imaging cameras. *J Nucl Med* 10: 197–201, 1969

12. ANGER HO: Scintillation camera with multichannel collimators. *J Nucl Med* 5: 515–531, 1964